Currents and fields reveal the propagation of nuclear polaritons through a resonant target

G. V. Smirnov,[1,*] U. van Bürck,[2] J. Arthur,[3] G. S. Brown,[4] A. I. Chumakov,[1,5] A. Q. R. Baron,[3,†] W. Petry,[2] and S. L. Ruby[3,‡]
[1]*Russian Research Center "Kurchatov Institute," 123182 Moscow, Russia*
[2]*Physik-Department, Technische Universität München, D-85748 Garching, Germany*
[3]*Stanford Synchrotron Radiation Laboratory, Stanford Linear Accelerator Center, Menlo Park, California 94025, USA*
[4]*Department of Physics, University of California Santa Cruz, Santa Cruz, California 95064, USA*
[5]*European Synchrotron Radiation Facility, F-38043, Grenoble, France*
(Received 20 February 2007; published 11 October 2007)

Nuclear resonant scattering of synchrotron radiation was investigated simultaneously in the spatially incoherent (4π) and in the spatially coherent (forward) scattering channels. A theory is presented which describes the main contributions to the scattering picture. To observe the 4π scattering, a nuclear target (spectator) was employed which was mounted downstream of another target (emitter). Emitter and spectator formed a combined scattering system. The time evolutions of the 4π scattering from the spectator and of the forward scattering from the combined system were measured and compared for different thicknesses of emitter and spectator. These observations and the analysis of the obtained time evolutions reveal how nuclear polaritons propagate through a scattering system.

DOI: 10.1103/PhysRevA.76.043811 PACS number(s): 42.50.Fx, 42.25.Hz, 61.10.Eq, 76.80.+y

I. NUCLEAR POLARITON

The existence of sharp resonances in the cross sections of nuclear reactions indicate the formation of relatively long-lived nuclear intermediate-state, compound nuclei. The formation of a compound nucleus is usually associated with the picture of a localized excitation. However, there are known processes in which a projectile interacts resonantly with a collection of nuclei, rather than with a single one. One example is the well-known phenomenon of neutron diffraction, where a single neutron is scattered coherently by a whole nuclear ensemble.

In this paper we consider an interesting class of nuclear resonance interactions that exhibits the properties of coherent scattering by a nuclear ensemble. This is the resonant absorption and emission of γ-ray photons by Mössbauer nuclei. This paper explores in detail how the coherent and incoherent scattering processes develop during multiple scattering of resonant photons by a macroscopic array of Mössbauer nuclei.

In Mössbauer absorption and emission, the interaction of γ-ray photons with nuclei is a *case of pure resonance scattering*, where the nucleus presents a simple resonating two-level system. The whole process of scattering can be divided into three stages: absorption of a primary γ quantum with formation of an intermediate excited state, dwelling in the intermediate state, and transition back to the ground state with emission of a secondary particle. The sharpness of the nuclear resonance corresponds to a long collision time, which is related to the lifetime of the nuclear excited state and lies for many Mössbauer nuclei in the range of $10^{-5}-10^{-9}$ s. Such conditions make it tempting to consider the interaction in terms of localization.

Indeed, the processes involved in traditional Mössbauer spectroscopy present interactions where the nuclear excitation is localized at individual nuclei. However, soon after the discovery of the Mössbauer effect, some experiments were performed which could not be understood in terms of the individual behavior of nuclei. First, there was the experiment of Lynch, Holland, and Hamermesh [1], where the propagation of a γ quantum through a target was correlated in time with its emission from a source. To find the proper description of the observed time dependences, the *scattering of the quantum by all nuclei* in the target had to be accounted for. In later experiments on total nuclear external reflection and on nuclear Bragg scattering (see, e.g., a review of the early experiments in Ref. [2]), it was necessary to take into account the *interaction of an individual* γ *quantum with the nuclear ensemble* in order to describe the observed scattering picture. Indeed, to understand diffraction one must consider the interference of all scattering paths, where, in each path, the quantum is scattered by an individual nucleus. That is, one must accept the existence of *internuclear interference* depending on the phase correlation between the individual paths. This is appropriate when there is no localization of interaction during the scattering process (such as nuclear spin flip or atomic recoil).

The concept of a delocalized nuclear excitation was introduced by Trammell [3] and Afanas'ev and Kagan [4]. The term *nuclear exciton* was coined by Zaretskij and Lomonosov [5].

In the case of elastic scattering of a γ quantum by a nuclear ensemble, where the intrinsic state of the scattering system is left unchanged, it is impossible to ascertain which nucleus in the ensemble was excited. Therefore, to account for the collective nuclear response, one has to assume an excitation probability for each nucleus in accordance with the quantum-mechanical principle of superposition of states. In the superpositional state the nuclear excitation is delocalized and thus the incident γ ray is shared by many nuclei. This is how the scattering process exhibits a collective character.

*smirnov@polyn.kiae.su
†Present address: SPring-8/RIKEN, 1-1-1 Kouto, Sayo, Hyogo, 679-5148, Japan.
‡Deceased.

 ©2007 The American Physical Society

The delocalized intermediate excited state created by a single γ quantum can be described as a spatially coherent superposition of N excited states:

$$\sum_{j=1}^{N} a_j \exp\{i\mathbf{k}\cdot\mathbf{r}_j\},$$

where in each contributing term of this sum one nucleus is excited with a definite probability amplitude a_j while all other nuclei are in the ground state. The spatial phasing of the excited nuclear currents over a system is determined by the spatial coherence of the field associated with the incident γ ray (in the above expression $\mathbf{k}$ is the wave vector of the incident radiation and $\mathbf{r}_j$ is the coordinate of the nucleus j). This superpositional state of nuclear excitations is called a nuclear exciton. *In the superpositional state each nucleus is excited with a certain probability amplitude*.

Nuclear excitation is related to a nuclear transition current. It is obvious that the latter cannot exist independently of the electromagnetic field. The two subsystems are united in a single physical entity. They interact with each other and exchange energy. Both propagate through the target as a coupled state of nuclear polarization and electromagnetic waves. At the exit of the target they generate a coherent radiation beam. The coupled system of nuclear currents and radiation field inside the target is called a *nuclear polariton*, by analogy to the collective molecular excitations known from optics (see, e.g., Ref. [6]). Recoilless nuclear scattering, a process preserving coherence, is responsible for creating and sustaining the nuclear polariton.

The aim of the present work was to study nuclear polariton propagation through a nuclear resonant target or in other words to study the temporal and spatial dynamics of nuclear polaritons in the process of nuclear forward scattering. In an earlier experiment, we pursued this aim by investigating the response of the coherent channel downstream of a target system at different target sequences [7]. In the present work we wanted in particular to study polariton propagation *at different depths in the target*. For this purpose two scattering intensities were recorded: the intensity of the spatially incoherent scattering (a probe of the nuclear excitation) and the intensity of the spatially coherent scattering in the forward direction (a probe of the propagating electromagnetic field).

In Sec. II, a brief description is given of incoherent scattering of synchrotron radiation (SR). Then in Sec. III a theory is presented which describes spatially incoherent scattering for the experimental model employed. In Sec. IV the measurements are described and the final data are presented, along with analysis and discussion.

II. SPATIALLY INCOHERENT SCATTERING CHANNELS

Each atom and nucleus has a probability for excitation by the primary field propagating through the target. They can then respond to the excitation in several ways (for example, by emitting secondary radiation), feeding several different scattering channels. The radiation elastically scattered in the direction of the primary beam builds up the coherent forward scattering channel. Secondary radiation scattered at other angles is spatially incoherent and forms a 4π shine around the target (we assume that the geometry does not permit Bragg diffraction). The 4π shine includes secondary radiation of different kinds: γ rays, electrons, fluorescence radiation, etc. Until now the time evolutions of the coherent and spatially incoherent scattering have been studied independently. Whereas studies of the nuclear forward scattering [8] have been performed by many authors and in different aspects [9,10], the time behavior of incoherent scattering has been analyzed only in a few theoretical [11–13] and experimental [13–16] papers. The incoherent channel is much less intense than the coherent one, making an experimental investigation of the time dependence of incoherent scattering rather troublesome. Moreover, the 4π shine presents a mixture of various scattering processes. Table I shows the most important contributions to the 4π shine. Both the nucleus and the atomic electrons contribute to the scattering.

We will begin by categorizing the various pathways to incoherent scattering of SR by a Mössbauer target, starting with those involving incoherent nuclear scattering. One can, for the sake of simple classification, divide the second-order process of nuclear resonant scattering into two stages: (a) absorption of the primary photon with simultaneous excitation of the nucleus and (b) decay of the excited nuclear state with emission of secondary particles. Because SR exhibits a broad energy spectrum, it can stimulate nuclear resonant excitation both without and with recoil (see the second column of the table).

Consider the case where a nucleus deep inside a sample is excited without recoil. This nucleus could be excited directly by the short SR pulse. Alternatively, because no recoil is involved, the nucleus could be excited by the precisely monochromatic coherent nuclear forward scattering (NFS) from nuclei upstream in the sample. The NFS represents the coherent sum of possible recoilless absorption and emission events in upstream nuclei, as was discussed above, and is delayed in time relative to the initial SR pulse. So one must consider the coherent superposition in time of both the prompt (X) and the delayed (γ_r) radiation, together giving rise to the excitation of our probe nucleus. This possibility is indicated by the two contributions in paths 1–3 of the recoilless absorption (see the third column of the table). One should notice that in this situation a typical nucleus sees an excitation field that includes both a prompt flash and thereafter a delayed field due to nuclear forward scattering by the upstream nuclei.

There are three possible ways for the excited nucleus to decay: (i) it can emit recoillessly a resonant γ-ray photon (γ_r), (ii) it can emit a γ-ray photon with recoil (γ_{nr}) (i.e., with simultaneous creation or annihilation of a lattice excitation: phonon=ph), and (iii) it can kick out an electron (e_c^-) from the atomic core in a process of internal conversion; the subsequent filling of the hole is accompanied by atomic fluorescence (X_{FL}) and possibly also the creation or annihilation of a phonon (ph). These three possibilities distinguish paths 1–3. Emission into 4π of a γ_r or γ_{nr} photon or conversion electron means the end of further forward scattering. The time dependence of any of these three scattering paths exhibits the time evolution of the nuclear excitation current driven by the propagating coherent field at the specific depth in the

TABLE I. Various paths of 4π scattering. The following abbreviations are used: X, the prompt part of radiation; it can be the initial SR pulse (third column) and the prompt x-ray radiation scattered by electrons (fourth column); γ_r, delayed resonant γ-ray photon coherently scattered by nuclei in the forward direction (third column) and a delayed resonant γ-ray photon emitted by a nucleus or scattered by an electron into 4π (fourth column); γ_{nr}, a delayed γ-ray photon emitted by nucleus with recoil, i.e., with simultaneous creation or annihilation of a lattice excitation: phonon=ph (fourth column); e_c^- and e_{ph}^-, electrons kicked out from the atomic core due to internal conversion and photoeffect; X_{FL}, fluorescent radiation, which is emitted while the hole in the atomic shell is being filled. See text for discussion.

Target	Kind of process	Incoming particles	Outgoing particles	Kind of process	Channel notation
Nucleus	Recoilless absorption	(1) $X+\gamma_r$	γ_r	Recoilless γ-ray emission	A
		(2) $X+\gamma_r$	$\gamma_{\mathrm{nr}}\pm\mathrm{ph}$	γ-ray emission with recoil	
		(3) $X+\gamma_r$	$e_c^-+X_{\mathrm{FL}}\pm\mathrm{ph}$	Internal conversion	
	Absorption with recoil	(4) $X\pm\mathrm{ph}$	γ_r	Recoilless γ-ray emission	B
		(5) $X\pm\mathrm{ph}$	$\gamma_{\mathrm{nr}}\pm\mathrm{ph}$	γ-ray emission with recoil	
		(6) $X\pm\mathrm{ph}$	$e_c^-+X_{\mathrm{FL}}\pm\mathrm{ph}$	Internal conversion	
Electron	Rayleigh scattering	(7) $X+\gamma_r$	$X+\gamma_r$	Elastic scattering	C
		(8) $X+\gamma_r$	$X+\gamma_{\mathrm{nr}}\pm\mathrm{ph}$	Inelastic scattering	
	Photoeffect	(9) $X+\gamma_r$	$e_{\mathrm{ph}}^-+X_{\mathrm{FL}}$	Elastic scattering	
		(10) $X+\gamma_r\pm\mathrm{ph}$	$e_{\mathrm{ph}}^-+X_{\mathrm{FL}}\pm\mathrm{ph}$	Inelastic scattering	

target. We will call the combination of these paths channel A.

Next, consider the case where the nucleus deep inside the sample is excited with recoil. This so-called phonon-assisted nuclear excitation is presented by paths 4, 5, and 6. The delayed coherent γ-ray field from the upstream part of the target has a precisely defined energy that does not allow it to excite a downstream nucleus with recoil. Thus, excitation with recoil can only be created by the initial SR flash itself. The nuclear excitation will then decay spontaneously either via emission of a resonant (γ_r) or a nonresonant (γ_{nr}) γ-ray photon or via emission of a conversion electron, accompanied by fluorescence radiation (X_{FL}). In the decay, a phonon can be created or annihilated. The time evolutions of paths 4–6 exhibit the decay of a free nucleus. These paths of absorption with recoil we will call channel B. Channel B has been used to great advantage for phonon spectroscopy, where it is known as nuclear inelastic scattering (NIS) [17–19].

In the presence of hyperfine splitting of the nuclear excited state, the time dependence in paths 1–6 can exhibit quantum beats (QBs). Experiments [15,16] have shown that the QB in paths 1 and 2 are best seen in optically thin targets where the coherent component γ_r of the exciting radiation is hardly developed, and hence the nuclei are not driven by the delayed radiation. In paths 4 and 5 the QB are seen for any thickness of the target. Exploiting path 5 has given rise to a method of perturbed angular correlation studies called synchrotron radiation perturbed angular correlations (SRPAC) [16] which is now fruitfully developing [20,21]. Similar QBs could be observed also by recording the time evolution of the e_c^- emission in paths 3 and 6.

Now we come to the paths where the electrons of the atomic shell perform the scattering [11–13]. The main feature of the interaction of radiation with electrons is that it is a prompt scattering (compared to the nanosecond time scale, which is of interest here). Therefore, unlike nuclear scattering, electronic scattering does not introduce interference in time; electronic scattering simply reproduces the time evolution of the incident radiation. The two main processes are Rayleigh scattering and photoelectric absorption. Rayleigh scattering can be elastic (seventh path) or inelastic (eighth path). In path 8 phonons participate in the scattering process. Photoabsorption is followed by the emission of electrons and of fluorescence radiation: see paths 9 and 10. In any of the electronic scattering paths the time distribution of the outgoing radiation (X, γ, or e_c^-) reproduces the time structure of the prompt pulse and that of the nuclear-delayed forward-scattered beam. The set of electronic scattering channels we call channel C.

In the experiment described in Ref. [13] time-dependent electron emission from iron foils excited by synchrotron radiation at the 14, 4-keV nuclear resonance of ^{57}Fe was observed. The delay between the absorption of a photon and the

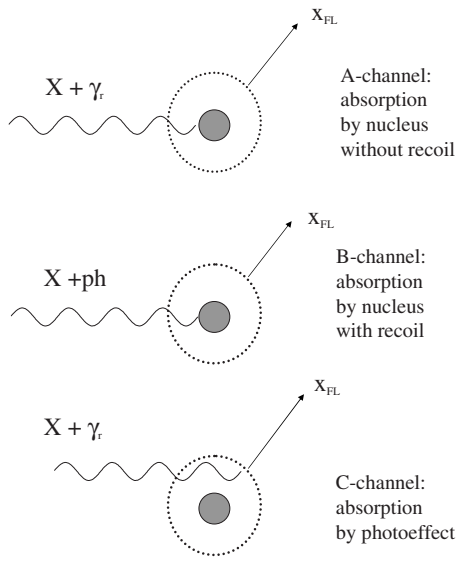

FIG. 1. Schematic view of the scattering channels considered in the theoretical analysis: *A*, nuclear recoil free absorption of the prompt SR pulse (X) and of the nuclear delayed radiation propagating in forward direction (γ_r); *B*, nuclear resonant absorption of the prompt radiation (X) with recoil; *C*, scattering the prompt SR pulse (X) and of the delayed nuclear radiation (γ_r) due to the photoeffect.

emission of the electron was of the order of the lifetime of the nuclear resonance—i.e., ~141 ns. The foils of different thicknesses were employed. The measured spectra were explained as the sum of the three *A*, *B*, and *C* contributions from different positions of the emitting nuclei on the track of the incident beam in the target. The authors did not touch yet the question of the space-time correlation between the 4π channels and the forward-scattering channel at the same depth. It is the goal of this work to investigate just this correlation and to reveal the propagation of a nuclear polariton through the target.

III. DETAILED THEORY

For our analysis of the 4π shine we select the dominant scattering paths, which are those where atomic fluorescence radiation X_{FL} is observed. The four selected scattering paths 3, 6, 9, and 10 of the table are displayed schematically in Fig. 1.

As mentioned above, only the recoilless scattering contributes to the formation and dynamics of the nuclear polariton. Therefore the contribution of this process to the 4π scattering is of special interest for our investigation of polariton propagation.

We briefly present a theory of spatially incoherent scattering adapted to our experiment. The approach is based on the theory developed in Ref. [12]. To find the contribution to each of the channels defined above, we shall use the response function technique. We denote the response function of a resonant nucleus by $g_n(t)$ and that of the electronic shell by $g_e(t)$. These functions have the following forms:

$$g_n(t) \propto \sigma_0 \exp\left(iw_0\tau - \frac{\tau}{2}\right)\Theta(\tau),$$

$$g_e(\tau) \propto \sigma_{ph}\delta(\tau), \tag{1}$$

where σ_0 and σ_{ph} are the nuclear resonance and photoelectric cross sections, respectively, w_0 is the dimensionless nuclear resonance frequency which equals $\omega_0 t_0$ (where ω_0 stands for the real resonance frequency and t_0 stands for the lifetime in the nuclear excited state), and $\tau = t/t_0$ is the dimensionless time with t as the real time. $\Theta(\tau)$ is the step function which is equal to unity at $\tau \geqslant 0$ and zero otherwise. The upper response function in Eq. (1) describes the delayed nuclear scattering, while the lower one describes the prompt electronic scattering. The amplitude of the propagating coherent field in the forward direction is given by the following expression [12,22]:

$$E(z,\tau) = E_0 \exp\left(-\frac{\mu_e z}{2}\right)\sqrt{\frac{1}{t_0}}\left\{\delta(\tau) - \frac{\mu_n z}{2}\exp\left(-iw_0\tau - \frac{q\tau}{2}\right)\sigma(\mu_n z\tau)\right\}, \tag{2}$$

with

$$\sigma = \frac{J_1(\sqrt{\mu_n z\tau})}{\sqrt{\mu_n z\tau}},$$

where J_1 is the Bessel function of the real argument and of the first order, z is the coordinate of the nucleus along the path of the propagating coherent field ($z=0$ at the entrance surface of the target), μ_n is the linear absorption coefficient of the radiation by the nuclei at resonance, μ_e is the electronic absorption coefficient, $E_0 = \sqrt{\frac{I_0}{\Delta w}}$ is the amplitude of the radiation field at the entrance of the scattering system with I_0 as the intensity of the SR within the frequency range Δw, the dimensionless parameter q describes the inhomogeneous broadening of the nuclear resonance in the target (which is assumed to preserve a Lorentzian shape: see Sec. 2.4.3 in Ref. [23]), and $q = 1 + \frac{\Delta\Gamma}{\Gamma_0}$, where Γ_0 is the natural linewidth and $\Delta\Gamma$ is an additional width of the resonance.

In accordance with the response function method the atomic response can be found as

$$A(\tau) = \int_{-\infty}^{\tau} d\tau' g(\tau - \tau')E(\tau'), \tag{3}$$

where A is the scattering amplitude, E is the amplitude of the driving field, and τ' and τ are, respectively, the excitation and the deexcitation times. In Fig. 2 the scattering geometry is displayed schematically. The incident synchrotron radiation is scattered initially by the upstream nuclear target (the emitter) in the forward direction. Radiation consisting of the prompt SR pulse and nuclear forward scattering with delay is incident on the downstream nuclear target (the spectator). Two detectors are used to record simultaneously the radiation scattered by the entire system into the forward direction (the NFS) and by the spectator into a small solid angle roughly perpendicular to the forward beam. It is quite clear that the smaller thickness of the spectator target is, the more adequate the spatial distribution of the nuclear polariton can be obtained. However, one has to find a compromise for the thick-

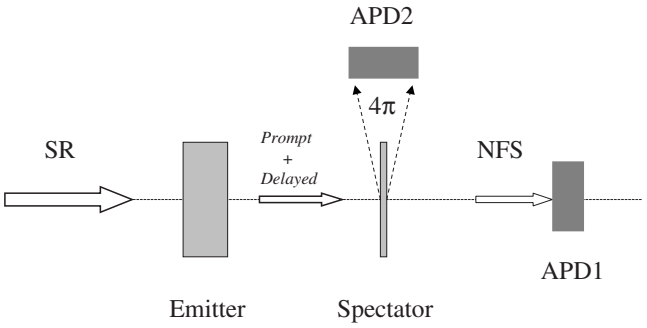

FIG. 2. Experimental layout. The nuclear target consists of two parts: emitter and spectator. The scattering intensity from the entire target in the forward direction (NFS) and that from the spectator at right angle to the propagating beam are recorded by the APD detectors APD1 and APD2, respectively.

ness to get sufficient scattering intensity in the incoherent channel.

We begin our analysis with the nuclear scattering channel denoted as channel A.

A. Channel *A*

In channel A emission must be preceded by recoil-free nuclear absorption of the *prompt SR pulse and of the delayed parts of the radiation propagating in the forward direction*. At a finite depth in the target a nucleus is illuminated initially by the SR pulse and then by the delayed γ radiation which is forward scattered by the nuclei in the upstream part of the target. This nucleus responds as a driven oscillator.

It is assumed that the single-line resonance in a target can be broadened, preserving the Lorentzian shape. The Lorentzian distribution of the resonance nuclear frequency w_0 has a half width $W=(q-1)/2$. The solution for the scattering amplitude by an individual nucleus j in the spectator target can be found directly in the time domain using the response function technique. Substituting in Eq. (3) the response function $g(\tau)=g_n(\tau)$ from Eq. (1) and the driving field $E(\tau)$ from Eq. (2) we obtain

$$A_j(z,\tau) \propto \int_0^\tau d\tau' \sigma_0 \exp\left[-i(w_0+\tilde{w})(\tau-\tau')-\frac{(\tau-\tau')}{2}\right] \times E_0 \exp\left(-\frac{\mu_e z}{2}\right)\sqrt{\frac{1}{t_0}}\left\{\delta(\tau') - \frac{\mu_n z}{2}\exp\left(-iw_0\tau'-\frac{q\tau'}{2}\right)\sigma(\mu_n z\tau')\right\}. \quad (4)$$

Now z is equal zero at the front of the emitter. The excited state in the spectator lasts for the time interval $(\tau-\tau')$. In the presence of an inhomogeneous distribution of nuclear resonances the value w_0 represents the average nuclear resonance frequency in the target and $w_0+\tilde{w}$ stands for the shifted resonance frequency of the scattering nucleus [in the case of hyperfine splitting one should use the expressions (36) and (37) in Ref. [12] for the scattering amplitude, where instead of the correlation function $F_s(\mathbf{k}_0,\tilde{\omega})$ an actual distribution of the resonance frequencies must be employed]. An immediate derivation yields the scattering amplitude

$$A_j(z,\tau) \propto E_0 \exp\left(-\frac{\mu_e z}{2}\right)\sigma_0 \exp\left(-i(w_0+\tilde{w})\tau-\frac{\tau}{2}\right) \times \sqrt{\frac{1}{t_0}}\left\{1-\int_0^\tau d\tau' \exp\left[i\tilde{w}\tau'-(q-1)\frac{\tau'}{2}\right] \times \frac{\mu_n z}{2}\sigma(\mu_n z\tau')\right\}. \quad (5)$$

The probability of scattering into the A channel at depth z $(d_e<z<d_s+d_e)$ can be found as the square modulus of the scattering amplitude which is averaged over the resonance energy distribution and summed over all resonant nuclei in the unit volume (the order of summing and averaging is arbitrary):

$$P(z,\tau) = \int \frac{d\tilde{w}}{\pi}\frac{W}{\tilde{w}^2+W^2}\sum_j |A_j(z,\tau,\tilde{w})|^2. \quad (6)$$

To pass from the scattering probability to the scattering intensity one has to perform integration over the spectator target thickness, d_s. Thus we arrive at the final expression for the scattering intensity into the A channel:

$$I^A_{4\pi}(\tau) = \frac{I_0}{\Delta w}\frac{\Gamma_e}{\hbar}N_r\sigma_0 f_{LM}\exp(-\tau) \times \int_{d_e}^{d_e+d_s} dz \exp(-\mu_e z)\int \frac{d\tilde{w}}{\pi}\frac{W}{\tilde{w}^2+W^2} \times \left|1-\int_0^\tau d\tau' \exp[i\tilde{w}\tau'-W\tau']\frac{\mu_n z}{2}\sigma(\mu_n z\tau)\right|^2, \quad (7)$$

where the preintegral factor is written explicitly for the case under consideration (hyperfine splitting is assumed to be absent). In the above expression Γ_e is the partial width of the nuclear level related to the process of internal electronic conversion, N_r is the number of resonant nuclei in the unit volume, f_{LM} is the Lamb-Mössbauer factor or recoilless factor in the target, and d_e is the emitter target thickness.

In the absence of resonance broadening no averaging over energy distribution is needed. Then the integral over time can be easily evaluated and Eq. (7) is reduced to

$$I^A_{4\pi}(\tau) = \frac{I_0}{\Delta w}\frac{\Gamma_e}{\hbar}N_r\sigma_0 f_{LM}\exp(-\tau) \times \int_{d_e}^{d_e+d_s} dz \exp(-\mu_e z)J_0^2(\sqrt{\mu_n z\tau}). \quad (8)$$

B. Channel *B*

As stated earlier, the energy distribution of the incident synchrotron radiation is large compared to the width of the phonon spectrum in the target, and therefore the nuclei can be resonantly excited with simultaneous creation or annihi-

lation of phonons. Only the broadband synchrotron radiation (the prompt pulse) can participate in these processes, not the narrow-band nuclear-scattered radiation. Therefore the amplitude of the exciting radiation can be expressed by $E_0 \exp(-\mu_e z/2)\sqrt{1/t_0}\delta(\tau)$, and for the scattering amplitude one obtains

$$A_j \propto \int_0^\tau d\tau' \sigma_0 \exp\left[-i(w_0+\tilde{w})(\tau-\tau')-\frac{(\tau-\tau')}{2}\right] \times E_0 \exp\left(-\frac{\mu_e z}{2}\right)\sqrt{\frac{1}{t_0}}\delta(\tau')$$

or

$$A_j \propto E_0\sqrt{\frac{1}{t_0}}\exp\left(-\frac{\mu_e z}{2}\right)\sigma_0 \exp\left[-i(w_0+\tilde{w})\tau-\frac{\tau}{2}\right]. \quad (9)$$

The scattering probability is given by the same expression as Eq. (6) where $|A_j(z,\tau,\tilde{w})|^2$ is a frequency-independent function now, so that the integral over $\tilde{w}$ is reduced to unity. Finally one arrives at the following scattering intensity into channel *B* from the spectator slab:

$$I^B_{4\pi}(\tau) = \frac{I_0}{\Delta w}\frac{\Gamma_e}{\hbar}N_r\sigma_0(1-f_{LM})\exp(-\tau)\int_{d_e}^{d_e+d_s} dz \exp(-\mu_e z), \quad (10)$$

which is a simple exponentially decaying function in time.

C. Channel *C*

Channel *C* is created by photoelectric absorption of the delayed coherent radiation propagating in the forward direction: paths 9 and 10 in Table I. The relevant atomic response function is given by Eq. (1). Using this function and the expression for the field, Eq. (2), one obtains for the scattering amplitude

$$A_j = \sigma_{ph}\int_0^\tau d\tau' \delta(\tau-\tau')E_0\exp\left(-\frac{\mu_e z}{2}\right) \times \sqrt{\frac{1}{t_0}}\left\{\delta(\tau')-\frac{\mu_n z}{2}\exp\left(-iw_0\tau'-\frac{q\tau'}{2}\right)\sigma(\mu_n z\tau)\right\}$$

or

$$A_j = E_0\exp\left(-\frac{\mu_e z}{2}\right)\sigma_{ph}\sqrt{\frac{1}{t_0}}\left[\delta(\tau) - \frac{\mu_n z}{2}\exp\left(-iw_0\tau-\frac{q\tau}{2}\right)\sigma(\mu_n z\tau)\right]. \quad (11)$$

The delayed scattering probability is

$$P(z,\tau) = |E_0|^2\frac{1}{t_0}\exp(-\mu_e z)\sigma_{ph}N\frac{(\mu_n z)^2}{4}\sigma^2(\mu_n z\tau)\exp(-q\tau), \quad (12)$$

where *N* denotes the number of both resonant and nonresonant atoms in a unit volume. Finally, the delayed scattering intensity from the spectator slab is

$$I^C_{4\pi}(\tau) = \frac{I_0}{\Delta w}\frac{\Gamma_0}{\hbar}\sigma_{ph}N\exp(-q\tau) \times \int_{d_e}^{d_e+d_s} dz \exp(-\mu_e z)\frac{(\mu_n z)^2}{4}\sigma^2(\mu_n z\tau). \quad (13)$$

In all the above expressions for the intensity, the common geometrical factor accounting for the transmission of fluorescence radiation to the detector is omitted.

D. Approximation for a thin target

Let us consider a single-target system where the target thickness d is small enough so that within a single nuclear lifetime $\tau<1$, the generalized space-time parameter $\mu_n z\tau \ll 1$. In this limit one can use the following approximations: $J_0(\sqrt{x})\approx\exp(-\frac{1}{4}x)$ and $\sigma(x)\approx\frac{1}{2}\exp(-\frac{1}{8}x)$. We substitute these exponential functions into Eqs. (7), (10), and (12) and take into account that $\Gamma_e=\alpha\Gamma_0/(\alpha+1)$, where α is the internal conversion coefficient, and $\mu_n=N_r\sigma_0 f_{LM}$, $\mu_e=\sigma_{ph}$N, where $\mu_n \gg \mu_e$. We assume $d_e=0$; then, we obtain for the *A*, *B*, and *C* contributions to the incoherent intensity

$$I^A_{4\pi}(\tau) \approx \frac{I_0}{\Delta w}\frac{\Gamma_0}{\hbar}\frac{\alpha}{\alpha+1}\mu_n\exp(-\tau) \times \int_0^d dz \exp(-\mu_e z)\exp\left(-\frac{1}{2}\mu_n z\tau\right),$$

$$I^B_{4\pi}(\tau) \approx \frac{I_0}{\Delta w}\frac{\Gamma_0}{\hbar}\frac{\alpha}{\alpha+1}\mu_n\frac{(1-f_{LM})}{f_{LM}}\exp(-\tau)\int_0^d dz \exp(-\mu_e z),$$

$$I^C_{4\pi}(\tau) \approx \frac{I_0}{\Delta w}\frac{\Gamma_0}{\hbar}\mu_e\exp(-q\tau) \times \int_0^d dz \exp(-\mu_e z)\frac{(\mu_n z)^2}{4}\frac{1}{4}\exp\left(-\frac{1}{4}\mu_n z\tau\right). \quad (14)$$

The integrals in the upper two equations equal approximately d (since one can approximate the exponentials by unity, their arguments being much less than unity). The integral in the lowest equation equals approximately

$$\int_0^d dz \exp(-\mu_e z)\frac{(\mu_n z)^2}{4}\frac{1}{4}\exp\left(-\frac{1}{4}\mu_n z\tau\right) \approx \frac{1}{16}\mu_n^2\frac{1}{3}d^3.$$

Finally we obtain

$$I^A_{4\pi}(\tau) \approx \frac{I_0}{\Delta w}\frac{\alpha}{1+\alpha}\frac{\Gamma_0}{\hbar}\mu_n d\exp(-\tau),$$

$$I^B_{4\pi}(\tau) \approx \frac{I_0}{\Delta w}\frac{\alpha}{1+\alpha}\frac{\Gamma_0}{\hbar}\mu_n d\frac{(1-f_{LM})}{f_{LM}}\exp(-\tau),$$

$$I^C_{4\pi}(\tau) \approx \frac{I_0}{\Delta w}\frac{\Gamma_0}{\hbar}\frac{1}{48}\mu_e d(\mu_n d)^2\exp(-\tau). \quad (15)$$

As seen from Eqs. (15), in this approximation each channel obeys an exponential time dependence. At all times τ the

ratio of the intensities in channels A and B is $I^A/I^B = I^A(0)/I^B(0) = f_{LM}/(1-f_{LM})$; i.e., it is strongly dependent on the recoilless factor. For thick targets the same ratios apply only for time $\tau=0$ [compare Eqs. (7) and (10)]. Thus, a high recoilless factor (which is, e.g., the case for a stainless steel target) causes the scattering intensity into channel A to greatly exceed that into channel B. The intensity ratio of the channels A and C for a thin target is at all times

$$\frac{I^C}{I^A} = \frac{I^C(0)}{I^A(0)} = \frac{1}{48}\mu_e d \frac{1+\alpha}{\alpha}\mu_n d,$$

i.e., it is much less than unity. Thus, in the approximation of a thin target channel A dominates the other two (B and C) in the whole time window. With an increase of the target thickness the contribution of channel C grows most rapidly, proportional to $(\mu_n d)^2$, and becomes dominant for thick targets.

E. Coupling of nuclear currents and fields in recoilless scattering

Figure 3 shows the distributions of the amplitudes of the nuclear excitation $A_j(z,t)$ and of the coherent field $E(z,t)$ inside of an arbitrary nuclear target at different times. A hypothetical single-resonance target characterized by a nuclear absorption cross section like that of ^{57}Fe was chosen for the evaluations. The nuclear excitation amplitude was calculated by using Eq. (5) for the case of a natural resonance width, where $\tilde{w} \equiv 0$ and $q=1$. In this case one obtains the following amplitude to find a nucleus in the excited state:

$$A_j(z,\tau) \propto \exp\left(-\frac{\mu_e z}{2}\right)\exp\left(iw_0\tau - \frac{\tau}{2}\right)J_0(\sqrt{\mu_n z \tau}), \quad (16)$$

where J_0 is the Bessel function of zeroth order.

The spatial and temporal evolution of the nuclear excitation amplitude (nuclear currents) is given by solid squares whereas that of the field is given by open circles. Field and nuclear currents are dynamically coupled: the prompt pulse of synchrotron radiation induces nuclear currents; in turn, the nuclear currents create their own field coupled with the nuclei. This coupling continues until the nuclear excitation vanishes. In this way the two subsystems of the nuclear polariton exchange energy, feeding each other.

At the bottom of Fig. 3, the distribution of the nuclear excitations and of the field created by them is shown at the very early time of ~1 ns after the passage of the prompt pulse. At this time the probability amplitude to find a nucleus in the excited state is roughly the same throughout the target. The amplitude of the created coherent field, by contrast, is linearly increasing with thickness. This corresponds to the *in-phase* addition of all the wavelets scattered by the individual nuclear layers in the forward direction.

The initial field created by the nuclei is coupled with the nuclei, causing the decay of the nuclear currents. So, at the time ~20 ns, the distribution of nuclear excitations is quite different. The probability amplitude to find excited nuclei near the exit of the target strongly drops down and equals zero at a depth of about 4 μm. By contrast, at the same thickness and at the same time the field amplitude reaches its maximum.

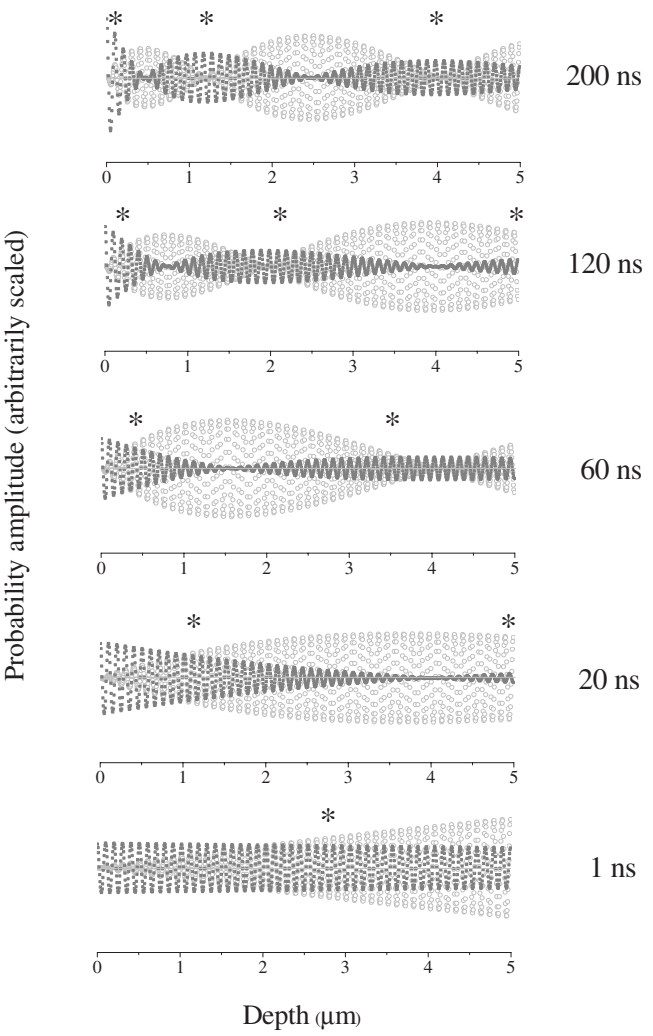

FIG. 3. Distributions of the probability amplitudes to find a nucleus excited (solid squares) and to find a resonant forward propagating γ-ray quantum (open circles) in a single-resonance nuclear target at different depths 0–5 μm and for different times 1–200 ns after excitation by the SR flash. The fast oscillations, which in reality occur with a period of the wavelength, have been included to aid in visualizing the wave packets. The envelope of the fast oscillations counts. Asterisks indicate the positions of maximum amplitude of the nuclear excitation.

Later on at about 60 ns, the picture is inverted: the probability amplitude of the nuclear excitation at this depth is growing again due to the pumping of energy from the field back to the nuclei, whereas the field amplitude drops to zero. This event can be interpreted as the second excitation of the nuclei in the target. A characteristic node-antinode structure is built up where the nodes of the nuclear currents coincide with the antinodes of the field. The number of nodes and antinodes is increasing with time (see, e.g., the panels for ~120 and ~200 ns).

These evolving spatial distributions of probability amplitude within the target can be used (a) to find where and when a γ-ray photon is likely to be present and (b) to find where and when an excited nucleus is likely to be present. The evolving distributions illustrate the temporal and spatial dy-

namics of a nuclear polariton in the process of nuclear forward scattering. This picture reflects also the dynamics of pumping of electromagnetic energy from the radiation field into the nuclear system and back during the propagation of a γ ray through the resonant medium. It is known from optics that in transient phenomena a relationship between the phase of the driving field and the driven dipole moments determines the direction of the energy exchange between the two systems. It is quite obvious that at the node points where the relative phase between radiation and nuclear dipoles is inverted (shifted by π) a transition between the regimes of emission and absorption of γ rays by the nuclei occurs. Thus, the space-time modulation of both the nuclear excitations and the propagating field reveals sequential processes of absorption and reemission of radiation by the nuclei. The increase of the number of nodes and antinodes should be interpreted as an increase of the number of scattering events inside the target. Multiple scattering occurs in thick targets and becomes apparent only after some time of interaction of the γ radiation with the nuclear ensemble (see the panels for increasing times). Figure 3 can be said to give a view of *when and where* [28] the γ-ray photon is absorbed by the nuclear ensemble during its propagation through the resonant medium.

IV. MODEL EXPERIMENT ILLUSTRATING WHEN AND WHERE NUCLEAR INTERACTION OCCURS

A. Instruments and measurements

The experiment was performed at Beamline 10-2 at the Stanford Synchrotron Radiation Laboratory. The storage ring was operated with only four electron bunches in the ring, giving a time delay of about 195 ns between successive x-ray pulses, each having a duration of about 0.2 ns. The x-ray pulses were generated by a multipole wiggler source, then filtered first by a grazing-incidence toroidal mirror (a low-pass filter with 22 keV cutoff, which also provided vertical collimation and horizontal focusing), then by a Si(111) monochromator, and finally by a narrow-band four-bounce monochromator using nested Si(422) and Si(10 6 4) channel-cut crystals [29]. This source provided about 10^7 photons/s at 14.4 keV in a bandwidth of about 10 meV, in a 3 mm (horizontal) by 1 mm (vertical) beam.

The x-ray detectors were large (10 mm diameter) avalanche photodiodes (APDs) [24]. They were capable of detecting single photons at both the 14.4 keV energy and also the 6.4 keV energy of Fe fluorescence. The detector electronics system was synchronized with the electron pulses in the storage ring, so that the delay time of detected x-rays could be measured with respect to the arrival of each x-ray pulse with an accuracy of about 2 ns. Occasionally during electron injection into the storage ring, extra small bunches of electrons were accidently injected into unintended orbits, giving false delayed signals. Care was taken to identify these spurious sources and eliminate them before taking data.

The scheme of the experimental setup is shown in Fig. 2, and its principle was already discussed in the theoretical section. The experiment used stainless steel foils ($Fe_{55}Cr_{25}Ni_{20}$) which were 95% enriched in ^{57}Fe. The foils were used singly or grouped together in combinations, giving effective foil thicknesses ranging from 2 to 28 μm. The x-ray beam first encountered a foil (or combination of foils) known as the *emitter* foil. After passing through these first foils, about 10 cm downstream the beam encountered another thin foil known as the *spectator* foil. All foils were rigidly mounted, normal to the beam path. One detector was placed just above the spectator foil, well out of the direct beam path, but only about 5 mm from the edge of the foil. This detector subtended a solid angle of about 1 sr as viewed from the center of beam impact on the foil. It collected the radiation that was scattered incoherently by the spectator foil. In particular, the detector recorded mainly 6 keV fluorescence radiation generated both by nuclear internal conversion in ^{57}Fe (paths 3, 6 in Table I) and by photoelectric absorption in the Fe, Cr, and Ni atoms (path 10). Another detector was located about 10 cm downstream of the spectator foil, in the direct beam path. This detector was used to collect the 14.4 keV radiation that was coherently scattered through both the absorber and the spectator foil.

The time distributions of the photons counted by the detectors were measured for various combinations of foil thicknesses. Both detectors were briefly overwhelmed by the intense flash of prompt (and promptly scattered) radiation associated with each x-ray pulse. Therefore, the counting electronics system was gated off for a few ns after each pulse. The precise pulse arrival time was checked periodically by heavily attenuating the x-ray beam and briefly removing the excluding gate signal.

B. Results and discussion

In Fig. 4 the complete set of the measured time distributions is presented: the forward scattering on the left-hand side and the corresponding 4π scattering on the right-hand side. Pronounced dynamical beats (DBs) of the forward-scattering intensity are seen in the left panels. This dynamical beating results from the exchange of energy between the nuclear ensemble and the γ-ray field [25–27]. This exchange process can be thought of as transitions between the different states of the nuclear polariton: a photon is absorbed and the nuclear ensemble is excited, or a photon is emitted and nuclei of the ensemble are in the ground state [7].

The number of DBs observed within the experimental time window (160 ns in our case) drastically increases with increasing thickness of the scattering system. Since the measurement senses the nuclei lying at the exit side of the target system, this means that the energy exchange between the field and nuclei becomes more and more frequent at greater depth into the target. One can see that at a depth of 2 μm in the target one exchange event is revealed within the experimental time window. At a depth of 8 μm in the target, two events are revealed during the same window, and at a depth of 26.5 μm in the target, five exchange events (i.e., transitions between the polariton states) are revealed. The results for the targets of 2 and 4 μm thickness correlate very well with the field amplitudes shown in Fig. 3 (imagine vertical lines at the relevant thicknesses in Fig. 3 and look for the open circles).

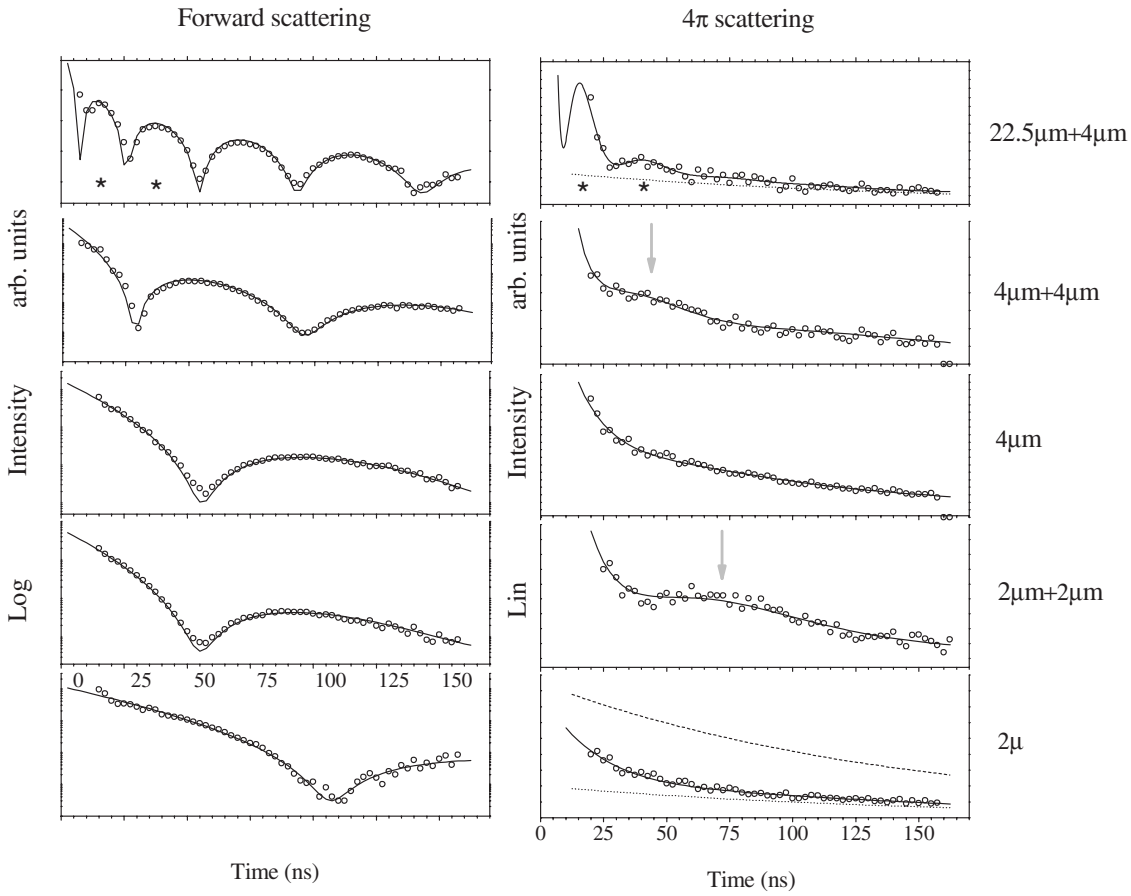

FIG. 4. The time evolutions of the forward scattering from different nuclear target stacks (emitter plus spectator) and of the 4π scattering from different spectator targets. Solid curves are fits of the experimental evolutions by the theory in accord with Eq. (2) for forward scattering and with Eqs. (8), (10), and (13) for 4π scattering, where the sum of all fluorescence contributions A, B, and C are taken into account. Dashed and dotted lines indicate exponential decay with a natural lifetime. Arrows indicate secondary nuclear excitation in scattering via channel A. Intensity bumps due to scattering via channel C are marked by asterisks.

The intensification of the energy exchange between the field and the nuclear currents with increasing target thickness can be understood if we remember that the strength of the coherent field is increasing proportionally to the thickness at the first instants after charging the nuclear ensemble by the SR pulse. It is important to remember that multiple transitions between polariton states occur only due to the recoil-free interaction of the radiation with the nuclei.

An additional, but different look at nuclear polariton development in space and time is offered by the 4π shine coming from a definite depth in the target. Whereas the NFS intensity reveals the amplitude of the radiation field at the exit, the nuclear 4π scattering intensity of channel A reveals the nuclear excitation currents at the space-time coordinate where the incoherent scattering occurs. As a spectator target we used either a 2-μm or 4-μm foil. For higher spatial resolution it would have been better to employ a thinner spectator foil, but the available SR intensity did not yield a sufficient signal from thinner spectator foils. Thus the 4π scattering was observed as an average over a thickness range of 2 μm or 4 μm. The bottom and middle panels on the right-hand side of Fig. 4 present the time dependence of the 4π scattering from each of these two spectator targets alone—i.e., in the absence of any emitter. During a time interval of about 0–50 ns (see the bottom panel) the decay of the 4π intensity and hence the nuclear deexcitation proceeds much faster than would a decay with natural lifetime. An exponential indicating natural decay is displayed in the same panel by a dashed line. At later times the deexcitation approaches the natural decay rate, which is given by a dotted curve for comparison. The accelerated decay of the nuclear excitation strongly indicates that the nuclear currents are driven by the field: at earlier times the field induces a faster nuclear deexcitation. The nonexponential decay of the nuclear excitation revealed by the 4π scattering is already clear evidence of the nuclear polariton dynamics in the target. A similar picture is observed in the middle panel for the 4-μm spectator.

Whereas the bottom panel reveals the nuclear excitation currents within the thickness range 0–2 μm, the panel above the bottom panel reveals the currents within the depth range 2–4 μm. In this case an emitter of 2 μm thickness was installed upstream of the spectator. A drastic transformation occurs now with the time behavior of the nuclear currents in the spectator: in the time interval from 40 to 120 ns a broad bump appears. It reveals the secondary nuclear excitation in

this time interval, at a depth of ~3 μm on average. This bump must be due to scattering channel *A* because (a) in scattering channel *B* the nuclei are excited only once by the prompt pulse at time zero and after this they decay monotonously and (b) the bump also could not appear due to channel *C*, since this channel should exhibit an intensity minimum within the relevant time interval at a depth of 3 μm (compare the locations of the minima of the NFS intensity for the 2-μm and 4-μm targets in the left panels). The coincidence of the observed maximum of the nuclear excitation current and of the minimum of the NFS intensity is in agreement with the correlation of the node-antinode patterns of field and nuclear currents predicted by the theory for the polariton propagation (see Fig. 3). Thus, the observed time distribution is a clear demonstration of nuclear polariton dynamics. Only the polariton mode can be responsible for the increase in intensity. The nuclear currents were initially excited by the SR flash at time zero, and later they were excited by the coherent field generated by the upstream layer within the time interval ~40–120 ns.

A similar polariton dynamics is revealed by the 4-μm spectator, illuminated by coherent radiation from a 4-μm emitter (see the second panel from the top on the right-hand side). The secondary excitation of the nuclear currents now occurs at earlier times: within the range ~25–75 ns. This is because the nuclei at a depth of 6 μm (the average depth here) exchange energy with the coherent field more frequently. Here the maximum of the nuclear excitation is less pronounced because it is partially hidden by the other scattering channels *B* and *C*, which become more influential with increasing thickness.

The next observation, presented in the top right panel, shows the dominance of scattering channel *C* deep into a thick target. Here the 4-μm spectator is illuminated by radiation from an emitter of 22.5 μm thickness. The observed bumps of the 4π intensity are now closely coincident in time with the bumps (marked by asterisk) seen in the forward scattering (see the top left panel). These bumps appear in the 4π channel due to scattering via channel *C*. However, at later times the time dependence is mostly exponential, as seen from the comparison with a pure exponential dependence (dotted line in the figure). This is evidence for channel *B* becoming dominant at these later times. In the next section we shall analyze the contributions of channels *A*, *B*, and *C* in greater detail.

C. Contributions to the 4π scattering

The quantitative relations of the different scattering contributions are strictly determined in the theory. Since the theoretical curves fit the experimental measurements well, it is worthwhile to decompose the latter into constituents corresponding to the different scattering channels. In this way one can distinguish the time evolutions of the different contributions and extract information about their roles in the summary picture for a given depth range in the target.

The time distributions of the 4π scattering from different depths in the target are presented in Fig. 5, where the total intensities are decomposed into three contributions originating from channels *A*, *B*, and *C*. The contribution of channel *A*, incoherent nuclear scattering involving recoil-free absorption of the prompt SR and of the nuclear delayed radiation, is displayed by the solid lines; the contribution of channel *B*, nuclear scattering involving absorption with recoil of the prompt SR, is displayed by the dashed lines; and the contribution of channel *C*, electronic scattering of the delayed nuclear radiation propagating in the forward direction, is displayed by the dotted lines.

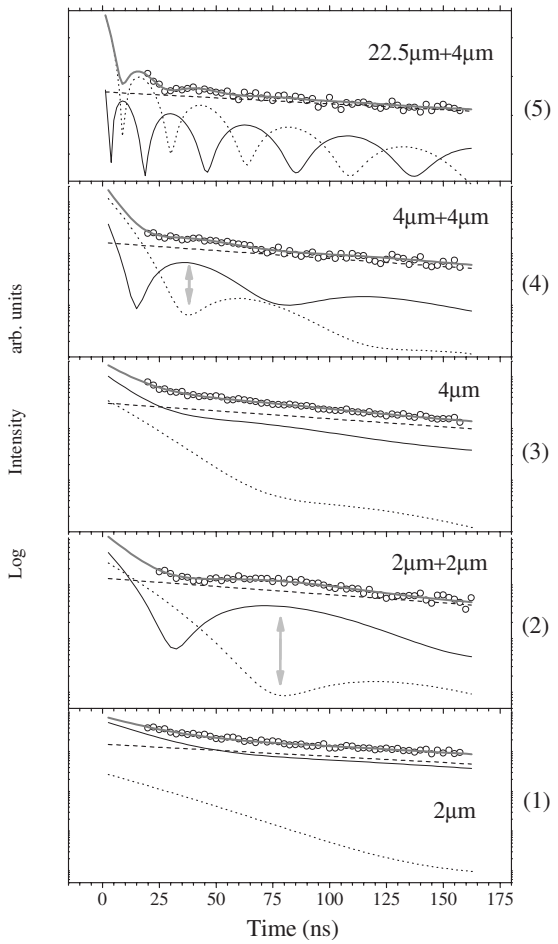

FIG. 5. Decomposition of the time evolutions of the 4π scattering from different spectator foils. The experimental evolutions are decomposed into the partial contributions from channel *A* (solid lines), channel *B* (dashed lines), and channel *C* (dotted lines) (see text). The summary intensity of the fit is given by the thick solid line. Arrows indicate secondary nuclear excitations in scattering via channel *A* and the relevant dips in scattering via channel *C*.

As discussed in Sec. II, the recoil-free scattering of the propagating radiation determines the formation of the polariton mode, where the excited nuclear currents and the propagating field are tightly coupled. Channel *A* reveals the time evolution of the nuclear currents excited by recoil-free absorption (we shall call them *A* currents), whereas channel *C* reveals the time evolution of the propagating field.

The time distribution measured with the 2-μm spectator alone, giving the response at an average depth of ~1 μm, is displayed in the panel (1) of Fig. 5. The accelerated decay of the *A* current is easily seen within the time interval of

$\sim 0-50$ ns at this depth. Within this interval the *A* current dominates. But because of its fast decay, it soon becomes comparable to the nuclear current excited with recoil: the *B* current. This happens already at ~ 50 ns. Both currents decay during later times, exponentially with natural lifetime.

At an average depth of ~ 2 μm [panel (3)], the accelerated decay of the *A* current proceeds in a shorter time interval $\sim 0-30$ ns and later drops far below the level of the *B* current.

The prominent feature seen in the other panels is the beat structure of the *A* and *C* time dependences, revealing the nuclear *A* current and the propagating field. The beating time structure is found within the depth ranges $\sim 2-4$ μm [panel (2)], $\sim 4-8$ μm [panel (4)], and $\sim 22.5-26.5$ μm [panel (5)]. At all depths the beating of the *A* and *C* time dependences proceed in opposite phase. This is characteristic of the nuclear polariton dynamics where the two subsystems, the nuclear currents and the field, exchange energy.

The signal from deep in the target is predominantly due to the scattering channel *C*—i.e., due to the electronic scattering of the delayed coherent field. The beat maxima in the total intensity observed in panels (2) and (4) are due to the nuclear currents, whereas the maxima seen in panel (5) are due to the field.

The signal from the *B* current always follows a natural decay. For thicknesses greater ~ 3 μm it becomes dominant in the second half of the time window.

V. CONCLUSION

This work examined the nuclear polariton, which is a coupled system of nuclear excitation currents and coherent γ-ray field inside a sample containing Mössbauer resonant nuclei. Evidence for the propagation of nuclear polaritons in targets of different thicknesses was obtained through the simultaneous detection of spatially incoherent scattering from varying depths in the target and of coherent scattering in the forward direction from the target.

The experimental data support a theory in which only the recoilless, coherent nuclear scattering is responsible for the formation and dynamics of the nuclear polariton.

The incoherent decay can be divided into three channels *A*, *B*, and *C*. Channel *A* reveals the time evolution of the nuclear currents excited by recoil-free absorption, whereas channel *C* reveals the time evolution of the propagating field.

In the approximation of a thin target, the single-nucleus scattering involving recoil-free absorption, channel *A*, dominates over the other channels throughout the whole time window. With increasing target thickness, the contribution of channel *C*, electronic scattering of the delayed coherent nuclear radiation, grows and becomes dominant.

ACKNOWLEDGMENTS

This work was supported by the Bundesministerium für Bildung, Wissenschaft, Forschung and Technologie under Contracts No. KS1WOC/2 and No. KS4WOC/3 and by the RRC Kurchatov Institute. Portions of this research were carried out at the Stanford Synchrotron Radiation Laboratory, a national user facility operated by Stanford University on behalf of the U.S. Department of Energy, Office of Basic Energy Science. The authors are grateful to E. E. Alp for the loan of the high-resolution monochromator.

[1] F. J. Lynch, R. E. Holland, and M. Hamermesh, Phys. Rev. **120**, 513 (1960).
[2] G. V. Smirnov, Hyperfine Interact. **27**, 203 (1986).
[3] G. T. Trammell, Proc. Intern. Atomic Energy Agency Symp. on Chem. Effects of Nucl. Transformations **1**, 75 (1961).
[4] A. M. Afanas'ev and Y. Kagan, JETP Lett. **2**, 81 (1965).
[5] D. F. Zaretskij and V. V. Lomonosov, Sov. Phys. JETP **21**, 243 (1965).
[6] C. Klingshirn, *Semiconductor Optics*, 3rd ed. (Springer, Berlin, 2006).
[7] G. V. Smirnov, U. van Bürck, W. Potzel, P. Schindelmann, S. L. Popov, E. Gerdau, Y. V. Shvyd'ko, H. D. Rüter, and O. Leupold, Phys. Rev. A **71**, 023804 (2005).
[8] U. van Bürck, D. P. Siddons, J. B. Hastings, U. Bergmann, and R. Hollatz, Phys. Rev. B **46**, 6207 (1992).
[9] *Nuclear Resonant Scattering of Synchrotron Radiation*, edited by E. Gerdau and H. de Waard (Baltzer Science, Bussum, 2000), Vols. 123-125 of Hyperfine Interact.
[10] Y. V. Shvyd'ko, Phys. Rev. B **59**, 9132 (1999).
[11] G. T. Trammell and J. P. Hannon, Phys. Rev. B **18**, 165 (1978).
[12] G. V. Smirnov and V. G. Kohn, Phys. Rev. B **52**, 3356 (1995).
[13] W. Sturhahn, K. W. Quast, T. S. Toellner, E. E. Alp, J. Metge, and E. Gerdau, Phys. Rev. B **53**, 171 (1996).
[14] U. Bergmann, J. B. Hastings, and D. P. Siddons, Phys. Rev. B **49**, 1513 (1994).
[15] A. Q. R. Baron, A. I. Chumakov, R. Rüffer, H. Grünsteudel, H. F. Grünsteudel, and O. Leupold, Europhys. Lett. **34**, 331 (1996).
[16] I. Sergueev, U. van Bürck, A. I. Chumakov, T. Asthalter, G. V. Smirnov, H. Franz, R. Rüffer, and W. Petry, Phys. Rev. B **73**, 024203 (2006).
[17] M. Seto, Y. Yoda, S. Kikuta, X. W. Zhang, and M. Ando, Phys. Rev. Lett. **74**, 3828 (1995).
[18] W. Sturhahn, T. S. Toellner, E. E. Alp, X. W. Zhang, M. Ando, Y. Yoda, S. Kikuta, M. Seto, C. W. Kimball, and B. Dabrowski, Phys. Rev. Lett. **74**, 3832 (1995).
[19] A. I. Chumakov and W. Sturhahn, Hyperfine Interact. **123/124**, 781 (1999).
[20] T. Asthalter, I. Sergeev, and U. van Bürck, J. Phys. Chem. Solids **66**, 2271 (2005).
[21] T. Asthalter, I. Sergeev, U. van Bürck, and R. Dinnebier, J. Phys. Chem. Solids **67**, 1416 (2006).
[22] Y. Kagan, A. M. Afanas'ev, and V. G. Kohn, J. Phys. C **12**, 615 (1979).
[23] G. V. Smirnov, Hyperfine Interact. **97/98**, 551 (1996).
[24] A. Q. R. Baron, Hyperfine Interact. **125**, 29 (2000).

[25] D. C. Burnham and R. Y. Chiao, Phys. Rev. **188**, 667 (1969).
[26] G. V. Smirnov, Hyperfine Interact. **123/124**, 31 (1999).
[27] U. van Bürck, Hyperfine Interact. **123/124**, 483 (1999).
[28] This was Stan Ruby's permanent and intricate question.
[29] T. S. Toellner, T. Mooney, S. Shastry, and E. E. Alp, Proc. SPIE **1740**, 218 (1992); T. Iskikawa, Y. Yoda, K. Izumi, C. K. Suzuki, X. W. Zhang, M. Ando, and S. Kikuta, Rev. Sci. Instrum. **63**, 1015 (1992).